A Wideband Spatial Channel Model for System-Wide Simulations

George Calcev, Dmitry Chizhik, Bo Göransson, Steven Howard, Howard Huang, Achilles Kogiantis, Andreas F. Molisch, Aris L. Moustakas, Doug Reed and Hao Xu

***Abstract*— A wideband space-time channel model is defined, which captures the multiple dependencies and variability in multi-cell, system-wide operating environments. The model provides a unified treatment of spatial and temporal parameters, giving their statistical description and dependencies across a large geographical area for three outdoor environments pertinent to third generation cellular system simulations. Parameter values are drawn from a broad base of recently published wideband and multiple antenna measurements. A methodology is given to generate fast-fading coefficients between a base station and a mobile user based on the summation of directional plane waves derived from the statistics of the space-time parameters. Extensions to the baseline channel model, such as polarized antennas, are given to provide a greater variety of spatial environments. Despite its comprehensive nature, the model's implementation complexity is reasonable so it can be used in simulating large-scale systems. Output statistics and capacities are used to illustrate the main characteristics of the model.**

I. Introduction

THE introduction of multiple antennas in the third generation cellular systems requires the detailed modeling of the spatial characteristics of the channel environment. Thus, the existing, widely-used, industry-standardized, temporal-only channel models [1]–[3] need to be extended so as to properly include the spatial domain. In the meantime, there has been a considerable number of publications on the topic of multiple-input multiple-output (MIMO) channel models. These can be grouped into two categories: (i) physical or scatterer-based models, which model the directional properties of the multipath components at the transmitter and receiver, and (ii) non-physical or correlation-based models, which model the transfer functions from each transmit to each receive antenna element, and the correlations between them.

In the first category, one can distinguish between, (a) generalizations of the tapped-delay-line and related approaches [4]–[11], which define the angular and delay distribution of radiation, and (b) geometry-based, stochastic models, which model the spatial distribution of scatterers and reflectors [12]–[20].

The non-physical models focus on the signal correlations at different antenna elements and typically assume correlated complex Gaussian fading. For different types of channels and complexity requirements, various models have been proposed, where the correlation matrix is, (a) the identity matrix [21], [22], (b) separable between transmitter and receiver [23]–[28], (c) a more general, non-separable matrix, with a particular approach of its representation as an eigenmode expansion, where the eigenspaces are identical at transmitter and receiver, is treated in [29].

The above-cited papers predominantly concentrate on flat-fading MIMO channels with no large-scale changes. The only existing comprehensive MIMO channel model, also formally defined by a cooperative effort of industry and academia, is the COST259 Directional Channel Model [30]–[33]. This model is very detailed, and thus also rather complicated. In particular, this model: *(i)* is a comprehensive model covering all kinds of radio environments, *(ii)* allows for the simulation of *continuous* large-scale changes of the mobile-station position, and *(iii)* is intended to be system-independent, i.e., to work for different carrier frequencies, and different system bandwidths. For that reason, it specifies a time- and angle continuous model. Also, a standardized model for *indoor* MIMO communications was recently finalized [34].

In [35] a hybrid model has been proposed to represent a general MIMO channel using a hybrid representation of the angular spectrum at the mobile and correlated fading at the base, once second order statistics, such as power delay and angular spectra are specified. The current work represents the MIMO channel as a superposition of clustered constituents, with stochastic powers, angles of departure and arrival, as well as times of arrival. Recommendations are made here on generation of second order statistical parameters based on both original and published results.

The industry consortia that develop the third generation standards (3GPP and 3GPP2) require the definition of widely accepted frameworks (e.g. channel environments and assumptions) on which to evaluate the proposed technologies. The work presented in this paper is the culmination of a joint effort by 3GPP and 3GPP2. The two standards bodies mandated the extension of the existing industry-adopted temporal models to provide a framework for a wideband, multi-antenna, system-wide simulation analysis. The finalized and adopted specification is described in [36].

The proposed model is intended for the three most com-

G. Calcev and D. Reed (GeorgeCalcev, Doug.Reed@motorola.com) are with Motorola, Schaumburg, IL. D. Chizhik, H. Huang, A. Kogiantis and A. Moustakas (chizhik, hchuang, achilles@lucent.com) are with Lucent Technologies, Murray Hill, NJ. B. Göransson (bo.goransson@ericsson.com) is with Ericsson Research, Stockholm, Sweden. S. Howard (showard@qualcomm.com) is with Qualcomm, San Diego, CA. A. Moustakas (arislm@phys.uoa.gr) was with Lucent Technologies when this work was submitted for publication, and is now at the National Capodistrian University of Athens, Greece. H. Xu (haoxu@ieee.org) was with Lucent Technologies when this work was conducted, and now is with Qualcomm, San Diego, CA. A. F. Molisch (Andreas.Molisch@ieee.org) is with Mitsubishi Electric Research Labs, Cambridge, MA, USA, and also with Lund University, Sweden.

mon cellular environments (as decided by the two standards bodies): suburban macrocells, urban macrocells, and urban microcells. The timeframe of the intended system simulations is assumed short enough, so that the model does not need to consider macroscopic terminal movement. The model is parameterized by the system bandwidth and is designed for bandwidths up to 5MHz. Therefore it is valid for most third generation systems, and it allows for performance comparisons between systems using different bandwidths. Furthermore, the channel model is specifically designed for multiple-antenna architectures at the base-station (BS) and/or at the mobile station (MS). Its herein description assumes linear antenna arrays, however it is straightforward to extend it to accommodate arbitrary array topologies. Finally, its structure seeks a balance between the realistic spatial environments and modeling complexity. Specifically, it generates a set of paths with discrete angles and delays. The generation of the channel coefficients for a system-level simulation is modular in structure and effort has been made to maintain a manageable computational complexity.

The rest of the paper is organized as follows: Section II describes the general structure of the model by means of definitions for the operating environment, the pathloss, and the correlation between the spatial parameters from different base stations, as well as generation of fast fading coefficients. In Section III, three extensions to the baseline channel model, and a model for polarized antennas, are given to represent a greater variety of common spatial environments. Finally, Section IV provides output statistics of the model and gives some insight into its behavior in terms of MIMO capacity metrics.

II. General Structure of Channel Model

This section describes the baseline spatial channel model and its implementation. The purpose of the model is to generate the channel coefficients between a given base station (BS) and mobile terminal (MS) based on a set of spatio-temporal parameters.

The statistical nature of the model is a feature that makes it particularly suitable for system-level analysis. The first step in the model is to choose one of three channel scenarios as described in Section II-A. Mobile users (MS) are dropped randomly in the area to be simulated. Note that in an actual system simulation, a large number of BSs and MSs may be modelled. However in describing the proposed channel model, we focus on a single BS/MS pair. Every BS-MS pair is a different realization of the channel conditions drawn from a common, system-wide, distribution. The model defines interactions of many BSs and many sectors to an MS using the site-to-site shadowing correlation. It does not define methods to model inter-cell interference since this is more of a simulation methodology issue than a channel model definition issue. Nevertheless the model defines all the necessary channel effects that would be needed for modeling inter-cell interference. Also, the model does not define channel model dependencies between MSs. Although correlation between MSs do exist (e.g. when MSs are co-located) the model does not include them since it would make the model less flexible. However, it is possible for the reader to add this functionality to the current channel model without violating any of the model's design approaches. The relationship between a given channel scenario and the channel coefficients for a BS/MS pair can be described in terms of three levels of abstraction.

At the macroscopic level, time-averaged local properties of the channel are described, e.g. the average power, delay-spread (DS) and angle-spread (AS). These quantities are also designated as "narrowband" parameters to imply the inclusion of all delayed components. Apart from a deterministic part, these variables have a log-normal random part, which captures the fluctuations due to propagation through several independent "city block" regions. These features are described in Sections II-C and II-D.

Focusing in to a deeper, "mesoscopic" level, the channel has additional structure (see Section II-E). In particular, each narrowband energy-cluster is decomposed into multiple paths with relative delays and angles of arrival (AoA) and departure (AoD) consistent with the narrowband statistics. Each of these paths can be thought of as coming from different buildings within the neighborhood of that block. Note that the above naming convention (AoD/AoA) corresponds to downlink channels, for signals originating at the BS and terminating at the MS. However, the full model is applicable also for uplink channels. Also at this mesoscopic level, the path delays and average path powers are generated as realizations of random variables. This is in contrast to the commonly used ITU models for link-level simulations (e.g., Pedestrian A or Vehicular A models, [1]) where these parameters are fixed. The proposed model is particularly well-suited for system-level analysis because its statistical nature more accurately reflects the wide range of user parameters found in actual systems.

At the deepest, microscopic level, each of these paths undergoes Rayleigh fading, generated from the temporal variability of the particular link (e.g. due to the terminal's movement). Each path is represented as a sum of sub-paths modelled as plane-waves (see Section II-F) .

Since the various length-scales are not always clearly separable, the interpretation of these levels of abstraction does not always correspond with reality. However, they certainly make sense and can always be used to describe the experimental data of outdoors channels.

A. Choosing a Channel Scenario

First a channel scenario is chosen, which defines a specific set of typical physical parameters of the environment. As mentioned in Section I, the analysis is limited to three general channel scenarios.

1) Suburban Macro: The suburban macrocell scenario describes a rural/suburban area with generally residential buildings and structures. The vegetation and any hills in the area are also assumed not to be too high. The base-station antenna position is high, well above local clutter. As a result, the angle-spread and delay-spread are relatively small. In addition, the base-to-base distance is approximately 3km.

2) Urban Macro: The urban macro-cellular environment describes large cells in areas with urban buildings of moderate

heights in the vicinity and significant scattering. The base-station antennas are placed at high elevations, well above the rooftops of any buildings in the immediate vicinity. The distance between base-stations is again about 3km. This scenario assumes moderate to high angle-spreads at the base-station and also large delay-spreads.

In urban environments, street canyon effects, i.e. wave propagation down relatively narrow streets with high buildings on both sides may be important in some cases and depending on their probability of occurrence, may lead to deviations from the generic urban macrocell case. Thus, street canyon effects are treated as optional extensions to the urban macro scenario. Details are discussed in Section III-C.

Another important effect, also treated as an option in this scenario, is the existence of additional clusters of energy due to far scatterers originating from high buildings. This is discussed in Section III-A.

3) Urban Micro: In contrast to the above scenario, the urban microcell scenario describes small urban cells with inter-base distances of approximately 1km. Base-antennas are located at rooftop level and therefore large angle-spreads are expected at the BS, even though the delay spread is only moderate.

In the case of macrocell scenarios discussed above, due to the relatively large area allocated to each base-station, the fraction of locations in the cell with the chance to have a line-of-sight (LOS) component from the base-station is small. Thus, for simplicity such channels are not modelled in the macrocell cases. However, for smaller cells, as in the case of microcell scenario, the users with LOS components cannot always be neglected. Thus, the way of including them is analyzed in Section III-B.

B. Dropping Users

Once the scenario has been chosen and the locations of the N_{BS} base-stations with the desired geometry and inter-base distances have been determined, one may start instantiating users in the area of interest. This entails first randomly generating the user locations. In addition, one needs to specify other user-specific quantities, such as their velocity vector $\mathbf{v}$, with its direction θ_v drawn from a uniform $[0, 360^\circ)$ distribution. Also, the specifics of the MS antenna or antenna array have to be determined, such as array orientation, Ω_{MS}, also drawn from a uniform $[0, 360^\circ)$ distribution, polarization, etc. Fig. 1 illustrates the various angle definitions.

It should be stressed that while the velocity of a particular MS is generally assumed to be non-zero, it is assumed here that the macroscopic and mesoscopic parameters do not vary over the duration of a simulation run. However, the velocity and position of the MS directly affects the microscopic parameters (e.g., the channel coefficients) as seen in Section II-F. This assumption does not allow the model to accurately treat the behavior of some users over the duration of a simulation ($\sim$minutes), since it does not describe dynamical hand-off situations or the passage of a particular user through different shadowing regions. However, it is expected that the statistics at a *system level* will not be affected.

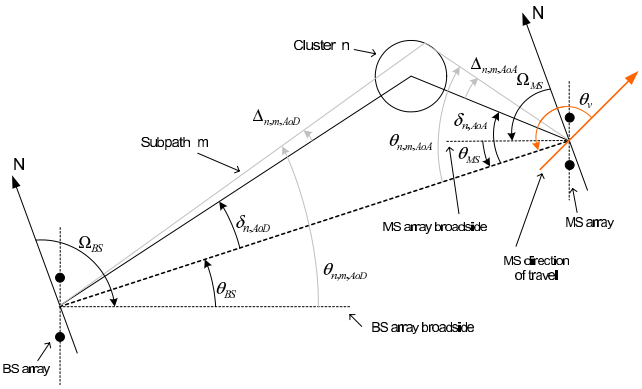

Fig. 1. Angular variables definitions

C. Pathloss

The following two pathloss models come from the widely accepted COST 231 models [37]. For a given user, the pathloss is a fixed multiplicative factor which is applied to all N multipath components described in II-E.

1) Suburban macrocell and urban macrocell environments: The macrocell pathloss is chosen to be the modified COST231 Hata urban propagation model, given by (4.4.1) in [37]:

$$\begin{aligned} PL[dB] \;=\; & (44.9 - 6.55\log_{10}(h_{BS}))\log_{10}\left(\frac{d}{1000}\right) \\ & +\; 45.5 + (35.46 - 1.1h_{MS})\log_{10}(f_c) \\ & -\; 13.82\log_{10}(h_{MS}) + 0.7h_{MS} + C \end{aligned} \tag{1}$$

where h_{BS} is the BS antenna height in meters, h_{MS} the MS antenna height in meters, f_c the carrier frequency in MHz, d is the distance between the BS and MS in meters, and C is a constant factor ($C = 0$dB for suburban macro and $C = 3$dB for urban macro).

Setting these parameters to $h_{BS} = 32m$, $h_{MS} = 1.5m$, and $f_c = 1900$ MHz, the pathloss formulas for the suburban and urban macro environments become, respectively, $PL = 31.5 + 35\log_{10}(d)$ and $PL = 34.5 + 35\log_{10}(d)$. The distance d is required to be at least $35m$.

2) Microcell environment: The microcell non-line-of-sight (NLOS) pathloss is chosen to be the COST 231 Walfish-Ikegami NLOS model, equations (4.4.6)-(4.4.16) in [37], with the following parameters: BS antenna height $h_{BS} = 12.5m$, building height $12m$, building-to-building distance $50m$, street width $25m$, MS antenna height $1.5m$, orientation 30° for all paths, and selection of metropolitan center. With these parameters, the pathloss formula simplifies to:

$$PL[dB] = -55.9 + 38\log_{10}(d) + (24.5 + \frac{f_c}{616.67})\log_{10}(f_c) \tag{2}$$

The resulting pathloss at 1900 MHz is: $PL(dB) = 34.53 + 38\log_{10}(d)$, where d is in meters. The distance d is assumed to be at least $20m$. It may be noted that the pathloss models adopted for the microcell and macrocell environments are quite similar for the parameters described above. A bulk log normal shadowing applying to all sub-paths has a standard deviation of 10 dB. The microcell LOS pathloss is based on the COST

231 street canyon model, given by (4.4.5) in [37]:

$$PL[dB] = -35.4 + 26\log_{10}(d) + 20\log_{10}(f_c) \qquad (3)$$

The resulting pathloss at 1900 MHz is $PL[dB] = 30.18 + 26\log_{10}(d)$, with f_c in MHz and d in meters and $d \geq 20$m. Log normal shadowing applied to all sub-paths has a standard deviation of 4 dB.

D. Generation of other Narrowband Parameters

In this Section the generation of shadowing coefficients is described, as well as the narrowband angle-spread and delay-spread and their cross-correlations. These will then be used in Section II-E to generate the mean angles of departure and relative delays of the intra-cluster sub-paths.

1) Narrowband Parameters for Macrocell Environments: The details of the generation of shadow-fading, angle-spread and delay-spread for the case of macrocell environments are described in this Section.

Shadow-fading fluctuations of the average received power are known to be log-normally distributed. Recently, for macrocell scenarios, the fluctuations in delay and angle spread were shown to behave similarly, [38]–[40]. The reason is that these quantities are sums of powers of individual sub-paths times the square of their corresponding delay times or angles. Since the powers are log-normally distributed and sums of log-normal variables are (approximately) log-normal [41], this implies that angle-spreads and delay-spreads have log-normal distributions. This explanation of the observed lognormal behavior of the delay spread was first conjectured in [38]. This motivation of how angle spread and delay spread are lognormally distributed also suggests that they will be correlated with shadow fading and each other.

Based on this log-normal behavior, the delay-spread $\sigma_{DS,n}$, BS angle-spread $\sigma_{AS,n}$ and shadow fading $\sigma_{SF,n}$ parameters of the signal from BS n, where $n = 1, \cdots, N_{BS}$, to a given user can be written as:

$$10\log_{10}(\sigma_{DS,n}) = \mu_{DS} + \epsilon_{DS}X_{1n} \qquad (4)$$
$$10\log_{10}(\sigma_{AS,n}) = \mu_{AS} + \epsilon_{AS}X_{2n} \qquad (5)$$
$$10\log_{10}(\sigma_{SF,n}) = \epsilon_{SF}X_{3n} \qquad (6)$$

In the above equations X_{1n}, X_{2n}, X_{3n} are zero-mean, unit-variance Gaussian random variables. μ_{DS} and μ_{AS} represent the median of the delay-spread and angle-spreads in dB. Similarly, the ϵ-coefficients are constants representing the log-normal variance of each parameter (e.g. $\epsilon_{DS}^2 = E\left[(10\log_{10}(\sigma_{DS,n}) - \mu_{DS})^2\right]$). The values of μ and ϵ for the two macrocell models appear in Table I. While there is some evidence [38], [39] that delay and angle spread may depend on distance between the transmitter and receiver, the effect on the system behavior is considered to be minor. Therefore, this dependence on the distance is not included here. Once $\sigma_{DS,n}$ and $\sigma_{AS,n}$ have been determined, they are used to generate the relative delays and mean angles of departure of the intra-cluster paths, see Section II-E.

Recent measurements have shown that for a given BS-MS pair, the various σ above are correlated [40], [42], [43]. In particular, $\sigma_{SF,n}$ is negatively correlated with $\sigma_{DS,n}$ and $\sigma_{AS,n}$, while the latter two have positive correlations with each other. It should be noted that this relationship does not hold for the angle-spread at the mobile since the different paths with distinct angles do not necessarily lead to such pronounced differences in the delays. These correlations can be expressed in terms of a covariance matrix $\mathbf{A}$, as seen in (7), whose A_{ij} component represents the correlations between X_{in} and X_{jn}, with $i, j = 1, 2, 3$.

Measurements of cross-correlations of these parameters between different base-stations are more sketchy. In particular, only correlations between shadow-fading components have been adopted [3], [44]. These correlations are assumed to be the same between any two different base-stations and are denoted by ζ. For simplicity and due to lack of further data, the cross-correlation matrix between the X_{in} triplet ($i = 1, 2, 3$) of different base-stations are assumed to be given by the following matrix $\mathbf{B}$

$$\mathbf{A} = \begin{bmatrix} 1 & \rho_{DA} & \rho_{DF} \\ \rho_{DA} & 1 & \rho_{AF} \\ \rho_{DF} & \rho_{AF} & 1 \end{bmatrix} \qquad \mathbf{B} = \begin{bmatrix} 0 & 0 & 0 \\ 0 & 0 & 0 \\ 0 & 0 & \zeta \end{bmatrix} \qquad (7)$$

with B_{ij} representing the correlations between X_{in} and X_{jm}, for $i, j = 1, 2, 3$ and $n \neq m$. The values chosen for these parameters are summarized below:

$$\begin{aligned} \rho_{DA} &= E\left[X_{1n}X_{2n}\right] = +0.5 \\ \rho_{DF} &= E\left[X_{2n}X_{3n}\right] = -0.6 \\ \rho_{AF} &= E\left[X_{3n}X_{1n}\right] = -0.6 \\ \zeta &= E\left[X_{3n}X_{3m}\right] = +0.5 \quad n \neq m \end{aligned}$$

For a given BS, the values of the cross-correlations ρ_{DA}, ρ_{DF}, ρ_{AF} above were chosen to be the rounded average of the measured parameters in [40]. The value of ζ is the adopted value between base-station shadow-fading parameters [3]. In addition, the choice of these values ensures that the triplet of X_{in} Gaussian random variables has a positive-definite covariance.

The random variables X_{in} can be generated with the above cross-correlations by first generating $3 + 1$ zero-mean unit-variance independent Gaussian random variables, namely Y_{in}, for $i = 1, 2, 3$ and $n = 1, \cdots, N_{BS}$, and Z_0. For a given MS, all its MS-BS links use independent Y_{in} triplets, but a common realization of Z_0. However, two different MSs should use independent Z_0 realizations. The X_{in} variables can then be written as

$$X_{in} = \sum_{j=1}^{3} C_{ij}Y_{jn} + \delta_{i3}\sqrt{\zeta}Z_0 \qquad \text{where} \quad \mathbf{C}^2 = \mathbf{A} - \mathbf{B} \quad (8)$$

and δ_{ij} is the Kronecker delta function. Note that since $\mathbf{A} - \mathbf{B}$ is positive-definite, the matrix square-root operation is well-defined.

2) Narrowband Parameters for Urban Microcell Environment: In the case of the urban micro-cellular environment, the fact that the base-station antennas are now positioned at rooftop level results to blurring the distinction between clusters and paths. This requires a different approach in dealing with delay and angle spread. Based on data by [40] and COST

TABLE I
ENVIRONMENT PARAMETERS

Channel Scenario	Suburban Macro	Urban Macro	Urban Micro
Number of paths	6	6	6
Number of sub-paths (M) per-path	20	20	20
Mean RMS AS at BS	$E(\sigma_{AS}) = 5^\circ$	$E(\sigma_{AS}) = 8^\circ, 15^\circ$	NLOS: $E(\sigma_{AS}) = 19^\circ$
AS at BS as a lognormal RV $\sigma_{AS} = 10^{(\epsilon_{AS} \cdot x + \mu_{AS})}$ $x \sim N(0,1)$ σ_{AS} in degrees	$\mu_{AS} = 0.69$ $\epsilon_{AS} = 0.13$	8° $\mu_{AS} = 0.810$ $\epsilon_{AS} = 0.34$ 15° $\mu_{AS} = 1.18$ $\epsilon_{AS} = 0.210$	N/A
$r_{AS} = \sigma_{AoD}/\sigma_{AS}$	1.2	1.3	N/A
Per-path AS at BS (Fixed)	2°	2°	5° (LOS and NLOS)
BS per-path AoD Distribution standard deviation	$N(0, \sigma^2_{AoD})$ where $\sigma_{AoD} = r_{AS} \cdot \sigma_{AS}$	$N(0, \sigma^2_{AoD})$ where $\sigma_{AoD} = r_{AS} \cdot \sigma_{AS}$	$U(-40^\circ, 40^\circ)$
Mean RMS AS at MS	$E(\sigma_{AS,MS}) = 68^\circ$	$E(\sigma_{AS,MS}) = 68^\circ$	$E(\sigma_{AS,MS}) = 68^\circ$
Per-path AS at MS (Fixed)	35°	35°	35°
MS Per-path AoA Distribution	$N(0, \sigma^2_{AoA}(Pr))$	$N(0, \sigma^2_{AoA}(Pr))$	$N(0, \sigma^2_{AoA}(Pr))$
Delay spread as a lognormal RV $\sigma_{DS} = 10^{(\epsilon_{DS} \cdot x + \mu_{DS})}$ $x \sim N(0,1)$ σ_{DS} in μsec	$\mu_{DS} = -6.80$ $\epsilon_{DS} = 0.288$	$\mu_{DS} = -6.18$ $\epsilon_{DS} = 0.18$	N/A
Mean total RMS Delay Spread	$E(\sigma_{DS}) = 0.17\mu s$	$E(\sigma_{DS}) = 0.65\mu s$	$E(\sigma_{DS}) = 0.251\mu s$ (output)
$r_{DS} = \sigma_{delays}/\sigma_{DS}$	1.4	1.7	N/A
Distribution for path delays			$U(0, 1.2\mu s)$
Lognormal shadowing standard deviation σ_{SF}	$8dB$	$8dB$	NLOS: $10dB$ LOS: $4dB$
Pathloss model (dB) d is in meters	$31.5 + 35\log_{10}(d)$	$34.5 + 35\log_{10}(d)$	NLOS: $34.53 + 38\log_{10}(d)$ LOS: $30.18 + 26\log_{10}(d)$

259 [42], the AoDs for the different paths follow a uniform distribution with a *fixed* width of 80° centered at broadside of the antenna(s) at the base-station. In addition, the individual path delays follow a uniform distribution between zero and $1.2\mu sec$, see Table I. Finally, the analysis of pathloss and shadowing is described in detail in Section III-B.

E. Generation of Wideband Parameters

In this Section the methodology of generating wideband parameters for each base-terminal link is presented. Its aim is to model the full wideband spatiotemporal channel response in a way that is both manageable from a complexity point of view and also quantitatively in agreement with measured properties of the channel, as described previously. Thus, a fixed number of paths $N = 6$, with distinct delays is generated, each with its own delay and mean AoD and AoA, consistent with the measured statistics. These N paths have a different interpretation in the macrocell and microcell environments, and thus these two cases will be treated separately below. In the former, the N paths collectively represent a single cluster of paths, leading to relatively small angular distances at the base. In contrast, in the latter case the N paths represent N distinct clusters, with large relative angular distances at the base.

1) Urban macrocell and suburban macrocell: Starting with the macrocell environments, we need to generate the characteristics of each of the N paths, namely their delays, power and mean AoD and AoA.

Path Delays: The random delays of the paths have been seen experimentally to follow an approximate exponential distribution [45]. Thus they can be expressed as

$$\tau'_n = -r_{DS}\sigma_{DS} \ln z_n \quad n = 1, ..., N \tag{9}$$

where z_n $(n = 1, ..., N)$ are i.i.d. random variables with uniform distribution $U(0,1)$ and σ_{DS} is derived in Section II-D. It should be emphasized that the time-scale for the generation of the delays τ'_n is generally not the same as that of the power delay profile given by σ_{DS} (and hence r_{DS}, signifying the ratio of the two time constants is not equal to unity). While σ_{DS} is related to the *power density* as a function of delay, $r_{DS}\sigma_{DS}$ is related to the *number density* as a function of delay and therefore should be larger than σ_{DS}, since the power is typically concentrated in the temporal domain [45]. For simplicity, r_{DS} is chosen to be a constant, independent of the particular realization of σ_{DS}. Its values are given in Table I.

The τ'_n variables are then ordered so that $\tau'_{(N)} > \tau'_{(N-1)} > ... > \tau'_{(1)}$. Then their minimum is subtracted from all, i.e. $\tau_n = \left(\tau'_{(n)} - \tau'_{(1)}\right)$, with $n = 1, ..., N$, so that $\tau_N > ... > \tau_1 = 0$.

Path Powers: There is sufficient experimental evidence that the power delay profile has an approximate exponential distribution [30], [45]. Thus, the average powers of the N paths can be expressed as

$$P'_n = e^{\frac{(1-r_{DS})\tau_n}{r_{DS} \cdot \sigma_{DS}}} \cdot 10^{-0.1\xi_n} \qquad n = 1, ..., N. \tag{10}$$

ξ_n for $n = 1, ..., N$ are i.i.d. Gaussian random variables with standard deviation $\sigma_{RND} = 3$dB, signifying the fluctuations of the powers away from the average exponential behavior. This parameter is also necessary to produce a dynamic range comparable to measurements, see [46]. Average powers are then normalized, so that the total average power for all N paths is equal to unity:

$$P_n = \frac{P'_n}{\sum_{j=1}^{N} P'_j}. \tag{11}$$

Angles of Departure (AoD): The spatial character of the adopted channel has a relatively large ($N = 6$) number of paths, each with a small angle spread (set to 2° in the macrocell case). This model would be quite accurate in the limit of many paths ($N \gg 1$), when the channel response approaches a continuum. For simplicity only $N = 6$ such paths are used. To satisfy the overall, narrowband angle spread of σ_{AS} described in the previous Section, the distribution of angles of departure at the BS has to be specified. For simplicity, a Gaussian distribution with variance $\sigma_{AoD} = r_{AS}\sigma_{AS}$ is chosen. The value of the proportionality constant r_{AS} is close to the measured values in [45] and is given in Table I. Higher values of r_{AS} correspond to power being more concentrated in a small AoD or a small number of paths that are closely spaced in angle. Thus the values of the AoD are initially given by

$$\delta'_n \sim N(0, \sigma^2_{AoD}), \tag{12}$$

where $n = 1, ..., N$. These variables are given in degrees and they are ordered in increasing absolute value so that $\left|\delta'_{(1)}\right| < \left|\delta'_{(2)}\right| < ... < \left|\delta'_{(N)}\right|$. The AoDs $\delta_{n,AoD}$, $n = 1, ..., N$ are assigned to the ordered variables so that $\delta_{n,AoD} = \delta'_{(n)}$, $n = 1, ..., N$.

Angles of Arrival (AoA): Similar to the case of AoDs, a model is necessary for the statistics of the AoAs at the MS. In data collected in a Chicago suburban environment, [47], it was observed that the paths that come from or close to the LOS tend to have higher relative power. The measurements showed that the AoA at the MS has a truncated normal distribution with mean zero with respect to the LOS, i.e.

$$\delta_{n,AoA} \sim N(0, \sigma^2_{n,AoA}), \tag{13}$$

with $n = 1, ..., N$. The variance of each path depends on the path's relative power. Based on the measured data, the variance $\sigma_{n,AoA}$ was found to depend on the relative power of that path as follows

$$\sigma_{n,AoA} = 104.12^\circ \cdot (1 - \exp(0.2175 \cdot P_{n,dBr})) \quad . \tag{14}$$

The $\sigma_{n,AoA}$ represents the standard deviation of the non-circular angle spread and $P_{n,dBr} < 0$ is the relative power of the $n - th$ path, in dBr, with respect to total received power. Fig. 2 illustrates the curve fit for the distribution of AoA obtained using uniformly spaced bins of the received power.

2) Urban Microcell : As discussed above, urban microcell environments differ from the macrocell environments in the way the paths are interpreted. In particular, since the individual multipaths correspond to separate clusters, they are independently shadowed. As in the macrocell case, $N = 6$ paths are modelled.

Path Delays: Since the N paths correspond to independent multipath components, their delays τ_n, $n = 1, ..., N$ are i.i.d. random variables drawn from a uniform distribution $U(0, 1.2\mu sec)$ (see chapter 3.2.4 in [42]). The minimum of these delays is subtracted from all so that the first delay is zero. When the LOS model is used, the delay of the direct component will also be set equal to zero.

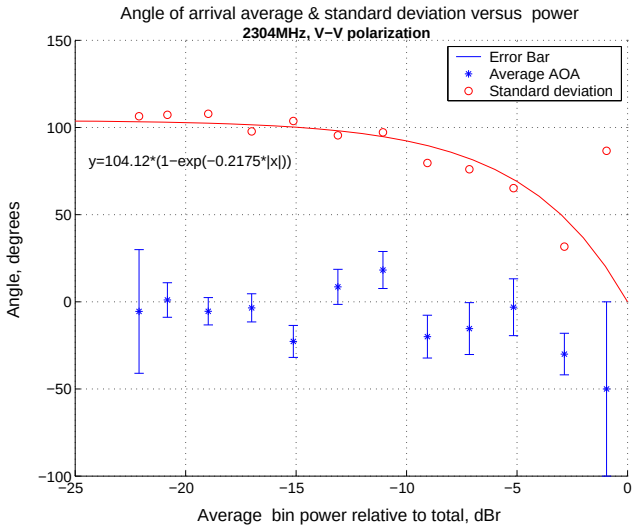

Fig. 2. Subscriber Angle of Arrival model

Path Powers: The power of each of the N paths should depend on the delay of each path. As in the macrocell case, it is natural to make the dependence negative exponential (see 3.2.4 in [42]), i.e.

$$P'_n = 10^{-(\tau_n + 0.1 z_n)} \tag{15}$$

where τ_n are the delays of each path in units of microseconds, and z_n ($n = 1, ..., N$) are i.i.d. zero mean Gaussian random variables with a standard deviation of 3dB. Average powers are normalized so that total average power for all N paths is equal to unity (11). When the LOS model is used, the normalization of the path powers has to include the power of the direct component P_D so that the ratio of powers in the direct path to the scattered paths is equal to K:

$$P_n = \frac{P'_n}{(K+1)\sum_{j=1}^{N} P'_j}, \; P_D = \frac{K}{K+1}. \tag{16}$$

Note that in the real world, a K-factor can be encountered even in channels that are NLOS. This would be the case when a dominant component is present. The default model here assumes the presence of Rayleigh fading only when not in LOS conditions.

Angles of Departure (AoD): In the microcell case each of the N paths is assumed to arrive from independent directions. As a result, their AoD at the base can be modelled as i.i.d. uniformly distributed random variables. For simplicity, the width of the distribution is kept finite, between -40 to +40 degrees:

$$\delta_{n,AoD} \sim U(-40^\circ, +40^\circ), \tag{17}$$

where $n = 1, ..., N$. One can now associate a power to each of the path delays determined above. Note that, unlike the macrocell environment, the AoDs do not need to be sorted before being assigned to a path power. When the LOS model is used, the AoD for the direct component is set equal to the line-of-sight path direction.

Angles of Arrival (AoA): The mean AoA of each path can be determined similar to the way discussed in the macrocell

TABLE II
SUB-PATH AOD AND AOA OFFSETS

Sub-path number (m)	Offset at BS, AS = 2°, Macrocell $\Delta_{n,m,AoD}$ (degrees)	Offset at BS AS = 5° Microcell $\Delta_{n,m,AoD}$ (degrees)	Offset at MS AS = 35° $\Delta_{n,m,AoA}$ (degrees)
1, 2	±0.0894	±0.2236	±1.5649
3, 4	±0.2826	±0.7064	±4.9447
5, 6	±0.4984	±1.2461	±8.7224
7, 8	±0.7431	±1.8578	±13.0045
9, 10	±1.0257	±2.5642	±17.9492
11, 12	±1.3594	±3.3986	±23.7899
13, 14	±1.7688	±4.4220	±30.9538
15, 16	±2.2961	±5.7403	±40.1824
17, 18	±3.0389	±7.5974	±53.1816
19, 20	±4.3101	±10.7753	±75.4274

case. In this case the AoAs are i.i.d Gaussian random variables

$$\delta_{n,AoA} \sim N(0, \sigma^2_{n,AoA}), \text{ where } n = 1, ..., N \quad (18)$$

$$\sigma_{n,AoA} = 104.12^\circ [1 - \exp(0.265 \cdot P_{dBr})] \quad (19)$$

and P_{dBr} is the relative power of the $n-th$ path in dBr. When the LOS model is used, the AoA for the direct component is set equal to the LOS path direction.

F. Generation of Fast-fading Coefficients

The methodology developed previously will now be extended for the generation of fast fading coefficients for wideband time-varying MIMO channels with S transmit antennas and U receive antennas. The fast-fading coefficients for each of the N paths are constructed by the superposition of M individual sub-paths, where each is modelled as a wave component. The $m-th$ component ($m = 1, \ldots, M$) is characterized by a relative angular offset to the mean AoD of the path at the BS, a relative angular offset to the mean AoA at the MS, a power and an overall phase. M is fixed to $M = 20$, and all sub-paths have the same power P_n/M. The sub-path delays are identical and equal to their corresponding path's delay. This simplification is necessary since the model has a limited delay resolution. The overall phase of each subpath $\Phi_{n,m}$ is i.i.d. and drawn from a uniform $[0, 2\pi)$ distribution. The relative offset of the $m-th$ subpath $\Delta_{n,m,AoD}$ at the BS, and $\Delta_{n,m,AoA}$ at the MS take fixed values given in Table II. For example, for the urban and suburban macrocell cases, the offsets for the first and second sub-paths at the BS are respectively $\Delta_{n,1,AoD} = 0.0894^\circ$ and $\Delta_{n,2,AoD} = -0.0894^\circ$. These offsets are chosen to result to the desired fixed per-path angle spreads (2° for the macrocell environments, 5° for the microcell environment for $\Delta_{n,m,AoD}$ at the BS and 35° at the MS for $\Delta_{n,m,AoA}$). These per-path angle spreads should not be confused with the narrowband angle spread σ_{AS} of the composite signal with N paths.

It is also required that the BS and MS sub-paths are associated, by connecting their respective parameters. While the $n-th$ BS path (defined by its delay τ_n, power P_n, and AoD $\delta_{n,AoD}$) is uniquely associated with the $n-th$ MS path (defined by its AoA $\delta_{n,AoA}$) because of the ordering, an explicit procedure must be defined for the sub-paths. It is thus proposed that for the $n-th$ path, randomly pair each of the M BS sub-paths (defined by its offset $\Delta_{n,m,AoD}$) with a MS sub-path (defined by its offset $\Delta_{n,m,AoA}$). Each sub-path pair is combined and the phases defined by $\Phi_{n,m}$ are applied. To simplify the notation, a renumbering of the M MS sub-path offsets with their newly associated BS sub-path is done. In other words, if the first $(m = 1)$ BS sub-path is randomly paired with the 10th $(m = 10)$ MS sub-path, then re- associate $\Delta_{n,1,AoA}$ (after pairing) with $\Delta_{n,10,AoA}$ (before pairing).

Summarizing, for the $n-th$ path, the AoD of the $m-th$ sub-path is

$$\theta_{n,m,AoD} = \theta_{BS} + \delta_{n,AoD} + \Delta_{n,m,AoD}, \quad (20)$$

from the BS array broadside. Similarly, the AoA of the $m-th$ sub-path for the $n-th$ path (from the MS array broadside) is

$$\theta_{n,m,AoA} = \theta_{MS} + \delta_{n,AoA} + \Delta_{n,m,AoA} \quad (21)$$

The antenna gains are dependent on these sub-path AoDs and AoAs. For the BS and MS, these are given respectively as $|\chi_{BS}(\theta_{n,m,AoD})|^2$ and $|\chi_{MS}(\theta_{n,m,AoA})|^2$, where $\chi(\theta)$ is the corresponding complex antenna response to and from radiation with angle θ.

Lastly, the path loss, based on the BS to MS distance and the log normal shadow fading, generated as described in Section II-E are applied to each of the sub-path powers of the channel model .

The channel transfer function between receiver u and transmitter s at path n and time t is determined by the superposition of a large number of sinusoidal sub-paths [35] as follows:

$$h_{u,s,n}(t) = \sqrt{\frac{P_n \sigma_{SF}}{M}} \sum_{m=1}^{M} \Big(e^{jk\|\mathbf{v}\| \cos(\theta_{n,m,AoA} - \theta_v)t} \chi_{BS}(\theta_{n,m,AoD}) \cdot e^{j(kd_s \sin(\theta_{n,m,AoD}) + \Phi_{n,m})} \chi_{MS}(\theta_{n,m,AoA}) \cdot e^{jkd_u \sin(\theta_{n,m,AoA})} \Big) \quad (22)$$

where, in addition to the earlier definitions

- k is the wave number $2\pi/\lambda$ where λ is the carrier wavelength in meters
- d_s is the distance in meters of the base station antenna element s from the reference $(s = 1)$ element. For the reference element $s = 1, d_1 = 0$.
- d_u is the distance in meters of the mobile station antenna element u from the reference $(u = 1)$ element. For the reference element $u = 1, d_1 = 0$.

(22) provides a simple expression to generate a time-dependent $U \times S$ channel matrix **H**(t) for a wideband MIMO system.

Measurements have shown that the elevation spread at the BS is much less than the azimuthal spread, [42]. For simplicity, this dependency is not included here. As mentioned in Section II, all channel parameters in (22) are time-varying at different time scales. The large-scale parameters, including power azimuth spectrum (PAS), power delay profile (PDP), AoD and AoA, are updated in each run of the simulation drop. The positional vector of the mobile is varying at the speed of the mobile, which leads to rapid phase changes in the sub-paths and the small-scale fading of the combined signal. It is also worth mentioning that the model's structure is flexible to

include joint distribution of PDP and PAS, but has not been considered in this paper. In fact, the PAS in (22), as well as the AoA and AoD can be functions of delay.

III. Additional Options

Beyond the main categorization of channels utilized in the previous Sections, often some special channel environments occur that cannot be adequately described with the above-developed models. Four additional special-case channel types are analyzed below and respective models are developed for each.

A. Far scatterer clusters

Signals arrive at the base station not only from the (approximate) direction of the mobile station, but also from other, separate regions of the delay/azimuth plane. These contributions correspond to radiation that is reflected or scattered at mountains, high-rise buildings, and other distinct geographical and morphological structures. This effect has been observed in many measurements, especially metropolitan areas that either have several high-rise buildings (published measurements collected in Frankfurt, Germany [48], [49]; Paris, France [50]; and San Francisco, USA [51]), or urban areas with interspersed unbuilt-up areas (e.g., Stockholm, Sweden [52]). The high-rise buildings can act either as specular reflectors, or as diffuse scatterers, depending on the building surface. In the following, the term "scatterers" will be used without loss of generality. For microcell environments, the propagation processes leading to far scatterers are somewhat different, where waves travel from the transmitter to the receiver via waveguiding. Different waveguides thus give rise to different clusters due to different propagation times and/or angles of incidence at the transmitter and receiver. The far scatterers lead to an increase of the angular spread as well as the delay spread of the arriving signal. It has been shown, e.g., in [53], that this leads to important changes in MIMO channel characteristics. Thus, far scatterer clusters are included as an option for this model.

The far scattering cluster (FSC) model presented here is a simplified model easily implemented in a system simulator, and containing the necessary elements to reproduce the key effects of the far scattering cluster. The model inserts three far scattering clusters in the cell area covered by each BS. Each FSC is then positioned randomly across the hexagonal area of service of the BS following the uniform distribution. The positioning process also imposes the constraint of the FSC being at least R=500m from the BS. Only the FSC which is closest to each MS is selected to be visible to that MS while the other FSCs in the cell are not present in the formation of that MS's channel model. The visible FSC then contributes paths to the MS's channel model, in addition to the default paths produced by the scattering around the MS. This approach makes use of FSCs in adjacent sectors when they are closer to the mobile than a FSCs in the serving BS. In this model, the three far-scatterers are independent of the BS antenna configuration or the number of sectors. The geometry shown in Fig. 3 is used to define several of the model parameters. The composite base angle spread associated with the NLOS

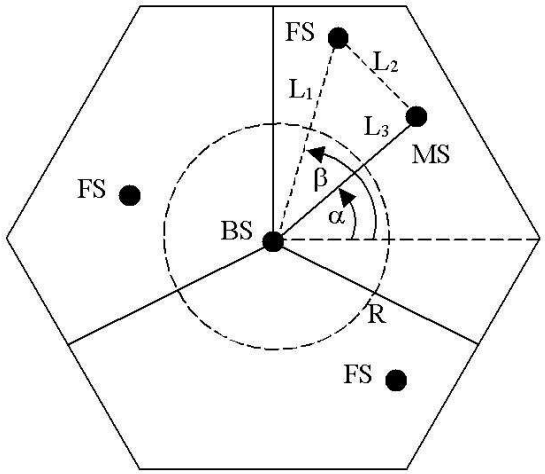

Fig. 3. Far-Scattering Cluster Geometry

propagation model will have an average AoD in the direction of α, and the individual path AoDs are simulated as in the urban macro-cell model. For the geometry defined by the FS, two of the N multi-path components are associated with the path to the FS, having a mean angle β, determined by the geometry of the FS location. Similarly, the path delays are defined by the distances, $L_1 + L_2$, the path distance from BS to MS via the FS, and L_3, the shortest path from BS to MS. The delays are specified by $\tau_{primary} = L_3/c_0$, and $\tau_{excess} = (L_1 + L_2 - L_3)/c_0$, where c_0 is the speed of light. The path delays and relative angles are chosen in the same way as for the primary path.

To implement the FSC model, the macro-cell channel model described in previous Sections is modified by applying the calculated excess delay and path loss to the two late arriving paths. The additional path loss of $1dB/\mu s$ is added with a $10dB$ maximum [32]. Before normalizing the path powers to unity, a site-correlated log normal shadowing $8dB/\sqrt{2}$ is applied to the two groups of multipaths associated with the primary path and excess path as defined above. The shadow fading has been observed to be common among paths of the same cluster, and different between clusters. A site-to-site correlation is used in this case since the environmental characteristics near the mobile are common to both paths producing correlated shadowing. A 50% correlation is assumed resulting in half the variance observed per cluster, i.e. the square root of two. After normalizing the path powers to unity, a final step of applying a common log normal shadowing random coefficient to all paths is performed similar to the macro-cell model.

When the Far Scatterer is added to the model with its extra path length, the delay spread is increased accordingly. The average value increases from the $0.65\mu s$ for the No-FS case to $0.98\mu s$ for the FS case. There is also an increased average angle spread caused by the relative angle difference and the powers associated with the signals arriving from the later cluster e.g. the nominal $AS = 15^\circ$ increases to 22.9°.

B. Micro-cell LOS modeling

Line-of-sight (LOS) paths occur when a direct "unobstructed" path exists between the base and subscriber. For micro-cells, LOS paths are typically present in combination with additional reflected paths producing canyon effects as described by the COST-Walfisch-Ikegami street canyon model [37]. This model results in a propagation slope modified from an ideal LOS path with an exponent of 2.0 to an exponent of 2.6, which is an empirical result based on measurements. LOS paths typically occur with greater probability when the subscriber is close to the base, where the path is more likely to be free of obstructions. At larger distances LOS conditions are typically more rare. These relationships are captured in the probability of occurrence of a LOS condition [30] given below

$$\text{Prob. of LOS} = \frac{300 - d}{300}, \text{ for } d \text{ (in meters)} < 300m \quad (23)$$

The micro-cell LOS model adds an additional LOS component, which is scaled in proportion to the scattered multi-path components to result in a K-factor, set [54] by the equation:

$$\begin{aligned} &\text{If (LOS)} : K = 13.0 - 0.03 \cdot d, \ K \text{ in } dB, d < 300m. \\ &\text{If (NLOS)} : K = -\infty \ dB \end{aligned} \quad (24)$$

When the LOS condition is selected, the Walfish-Ikegami street canyon model [37] is used as the propagation loss model, with the simplified equation as specified in (3). A log normal shadow fading $\sigma_{SF} = 4dB$ is chosen to represent the variations seen in the LOS street canyon environment.

When the NLOS condition is present, the Walfish-Ikegami micro-cell model [37] is selected, with some simplifications (for a typical street environment and average angle of propagation), as described in (2). The log normal shadow fading is $10dB$ for the NLOS path loss model.

By including a LOS path in the model, a reduction in average AS and average DS is produced since the stronger direct component occurs at zero degrees and zero delay with respect to the MS. In addition, significantly more of the lower values of AS and DS (after the addition of the LOS component) occur than for the strictly NLOS case. These low values represent cases that are more highly correlated.

C. Urban Canyon Modelling

Street canyon effects, consisting of several propagation mechanisms can be found in dense urban areas where signals propagate between building rows. In canyons, received signals typically contain multiple delayed paths arriving from similar angles and having narrow angle spreads. Environment-specific effects are evident [50], with some locations having first arriving paths from over-rooftop propagation and later paths arriving from down the street. In other locations, down the street paths are the dominant effect, where path AoAs are all similar. Since these effects vary with location, a simplified model was created to simulate urban canyon effects without the need for defining building grids.

When the paths arriving at the subscriber are confined to a narrow set of AoAs, the correlation between subscriber antennas is typically at its highest. This is an important situation to test in a multi-antenna study. To emulate the canyon effect, a channel generating parameter α is defined and used to set the probability of obtaining all paths coincident in angle of arrival at the subscriber. The value of α was selected to be 90% as a preferred value to emphasize the occurrence of the common angle of arrival. For the remaining 10%, the standard power dependent angle of arrival model is used at the subscriber. This model will produce composite $AS = 35^\circ$ (the per-path angle spread) with a 90% occurrence, and for the remaining 10% a value ranging from 35° to about 100°.

D. Polarization Propagation: Modelling and parameters

Usually channel models analyze only the propagation of vertical polarization, corresponding to the transmission and reception from vertically polarized antennas. Recently antenna architectures with cross-polarized antennas have been considered. Therefore, it is necessary to model the propagation and mixing of dual-polarized radiation. To be consistent with previous models, only propagation in the two-dimensional (horizontal) plane will be considered. Therefore, it is natural to split the radiation into two components, namely vertically and horizontally polarized radiation. The transmission from a vertically polarized antenna will undergo scattering resulting to energy leaked into the horizontal polarization before reaching the receiver antenna. By employing two co-located antennas at the receiver with orthogonal polarizations the total received signal power will be higher from that of a single vertically polarized antenna.

In the remainder of the Section, polarized antennas will be defined as structures that receive or transmit at one polarization. Whatever the implementation of a polarized antenna might be, the definitions and modeling to follow will assume that an equivalent response on a two-dimensional plane can be defined, which can be fully characterized by its decomposition into the two orthogonal axes: Vertical, (V), and Horizontal, (H). Polarized antennas will be used for transmission or reception at the BS or at the MS.

The channel phenomena appearing in multi-polarization transmission can be categorized in three areas:

- Power Delay Profile (PDP). The PDP can be analyzed on a per path and polarization basis. The delays of two polarizations for a given path coincide in time. The average path powers of the horizontal and vertical polarizations assuming the transmission from e.g. a vertically polarized antenna are generally unequal. [55]–[58]. The Cross-Polarization-Discrimination, XPD, is a typical figure of merit used in characterizing the mean power transfer from one polarization to another. It is defined as $XPD = P_{V-V}/P_{V-H}$, which assumes that the transmission originates in the V polarization and the receiver observes power P_{V-V} in the V orientation versus P_{V-H} in the H orientation. Also, XPD is not necessarily identical between paths. Statistical descriptions on the variability of the XPD between paths has been reported and will be used here.
- Spatial Profile. When comparing the per path spatial behavior between two polarizations, there is no conclusive

studies that show in what manner they could be different. Thus, in the absence of any data, the rms per path AS and the mean per path AoD/AoA are assumed to be identical for the respective paths between the two polarizations.

- Symmetry. No conclusive studies exist supporting that the H originated transmission should have different statistics than the V one. Thus, for simplicity it is assumed that the two types of coupling exhibit identical XPD statistics while having independent XPD instantiations for each polarization.

1) Polarization Measurement Data: The polarization measurements available in the literature can be categorized by the type of environment in which they were obtained. Macrocells tend to exhibit different XPD statistics (i.e. first and second order moments) than microcells due to the significant difference in the amount of scattering, [59]. Although XPD models have been proposed based on semi-analytical approach, such as in [60], here the effort is to base the model on measurement data. The XPD was measured in the same measurement campaign as the angle-of-arrival in the Chicago suburbs (Schaumburg), [61], using V and H polarized antennas at both ends. Fig. 4 describes the ratios of P_{V-V}/P_{V-H} and P_{V-V}/P_{H-V}. The XPD shows a linear dependence with path power with a $5.2dB$ standard deviation with respect to the linear regression. As seen in Fig. 4, the median value of XPD is dependent on the mean relative power of the measured path. For example, if the power is confined to a single path, i.e. $0dBr$, the median XPD is approximately $7dB$. For weaker paths, e.g. $-20dBr$, the median XPD is approximately $0dB$. During its propagation an electromagnetic wave (ray) would suffer several parallel and oblique reflections, and diffractions that change its polarization and decrease its power. One expects that the more scattering a wave suffers,

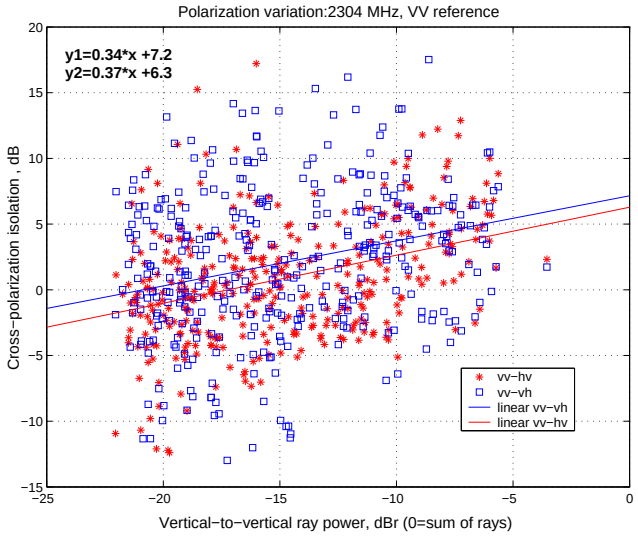

Fig. 4. XPD versus path (ray) power

the more mixing its polarization will undergo and the weaker its power will become. Therefore, it is expected that both the cross-polarization discrimination (XPD) and the wave power will decrease considerably after a number of random reflections. For modeling purposes XPD random realizations, independent for each path, are drawn for urban macrocell and microcell, as shown below:

$$P_{V-H} = P_{V-V} + A + B \cdot N(0,1) \tag{25}$$

Urban Macro: $A = 0.34P_{n\_dB} + 7.2dB$, $B = 5.5dB$
Urban Micro: $A = 8dB$, $B = 8dB$

where a V polarization is assumed for transmission, $P_{n\_dB} < 0$ is the mean relative path Power P_n in dBr, and B corresponds to the lognormal standard deviation of the XPD draw.

2) Channel Coefficients for Polarized Antennas: An extension to the model in Section II-F is defined.

$$\begin{aligned} h_{u,s,n}(t) = \sqrt{\frac{P_n \sigma_{SF}}{M}} \sum_{m=1}^{M} \Bigg(& \begin{bmatrix} \chi^v{}_{BS}(\theta_{n,m,AoD}) \\ \chi^h{}_{BS}(\theta_{n,m,AoD}) \end{bmatrix}^T \\ & \times \begin{bmatrix} e^{j\Phi_{n,m}^{(v,v)}} & \sqrt{r_{n1}} e^{j\Phi_{n,m}^{(h,v)}} \\ \sqrt{r_{n2}} e^{j\Phi_{n,m}^{(v,h)}} & e^{j\Phi_{n,m}^{(h,h)}} \end{bmatrix} \times \begin{bmatrix} \chi^v{}_{MS}(\theta_{n,m,AoA}) \\ \chi^h{}_{MS}(\theta_{n,m,AoA}) \end{bmatrix} \\ & \times e^{jkd_s \sin(\theta_{n,m,AoD})} \times e^{jkd_u \sin(\theta_{n,m,AoA})} \\ & \times e^{jk\|\mathbf{v}\| \cos(\theta_{n,m,AoA} - \theta_v)t} \Bigg) \end{aligned} \tag{26}$$

where

- $\chi^h_{BS}(\cdot)$ is the base station complex antenna response in the H polarization. The squared norm of the antenna response $\|\chi(\cdot)\|^2$ is the real valued antenna gain. The other χ's are defined similarly.
- r_{n1} is defined as the inverse of the random variable drawn from (25) for the $n-th$ path, $r_{n1} \triangleq \frac{1}{XPD}$. An independent XPD value is assigned for each path. The corresponding random variable for the $(H-V)$ versus the $(V-V)$ ratio is defined as r_{n2}.
- $\Phi_{n,m}^{(h,v)}$ is the initial random phase of the m^{th} subpath in the n^{th} path that originates in the H direction and arrives in the V direction. Each initial phase is drawn independently under the assumption that the fast fading for each antenna and polarization pair combination is assumed independent of the others.

Equation (26) defines the channel realization between a pair of antennas. The antennas are elements positioned in some generic direction in a two-dimensional plane so that their responses can be decomposed into V and H. Thus, each antenna response is a 2×1 complex vector. The 2×2 matrix defines the coupling in terms of scattering phases and amplitudes of all four combinations of the two transmit and two receive decompositions. It should be stressed that the correlations between antennas resulting from this form of channel can no longer be written in the form of a Kronecker matrix product of correlations of the transmitter and receiver arrays. Instead, they can be written as sums of such matrix products, with each product representing the correlations for a certain mode (e.g. $V-H$, $H-H$, etc).

IV. Simulated Model Statistics

The wideband model developed in Section II specifies also the system-wide spatio-temporal profile, beyond the point-to-point channel characterization. Thus, all resulting output

statistics from the model are presented in terms of cumulative distribution functions. The illustration of the resulting narrowband rms delay spread for the three environments using the parameters of Table I are given in Fig. 5 along with the targeted CDFs obtained from the measurements. Similarly, the same family of quantities for the narrowband rms angle spread observed at the base is shown in Fig. 6.

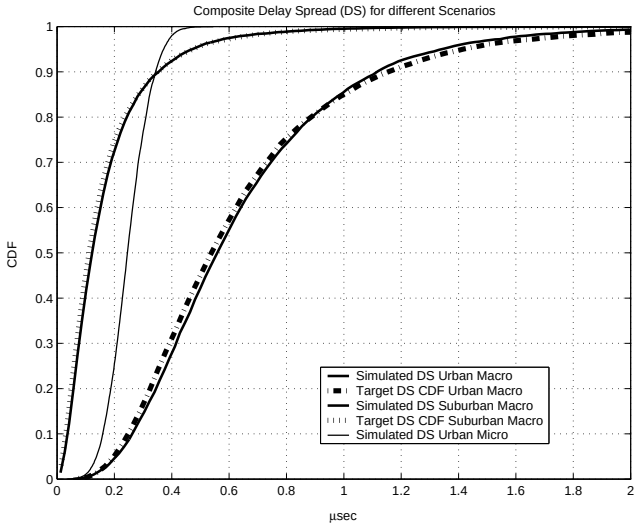

Fig. 5. Simulated and measured CDFs of Delay Spread for the three environments

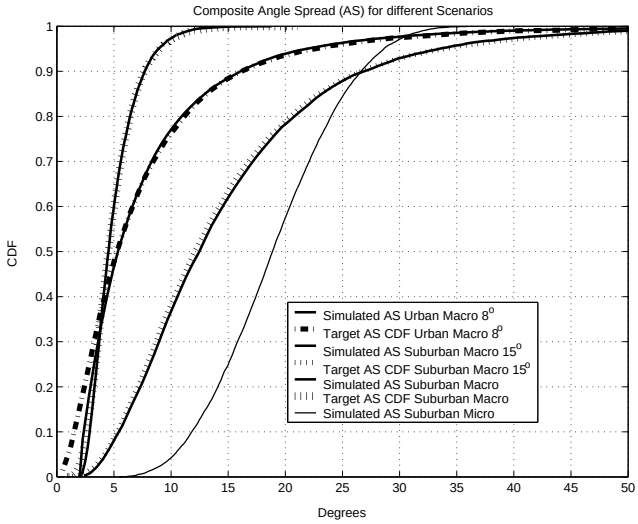

Fig. 6. Simulated and measured CDFs of Angle Spread for the three environments

Also, MIMO performance is evaluated for different MIMO BS and MS configurations and different channel environments. Significant correlation is necessary before capacity is reduced from uncorrelated, random channel matrix results. Wideband $U \times S$ MIMO capacity for a Suburban macrocell, Urban macrocell, and Urban microcell environments are evaluated using the Spatial Channel Model specified here. A simple case of beamsteering is also included to compare the performance of the multi-stream MIMO capacity metric to that of a single stream, which should perform well for correlated environments. For simplicity, and to minimize feedback information, the single stream is beamformed to the LOS angle of departure of the user, θ_{BS}, which here is assumed to be $\theta_{BS} = 0$.

For the $U \times S$ channel matrix $\mathbf{H}$ the capacity, C, [22], is:

$$C = \log_2 \left(\det \left[\mathbf{I} + \frac{\rho}{S} \mathbf{H}\mathbf{H}^\dagger \right] \right) \qquad \text{bps/Hz} \qquad (27)$$

where $\mathbf{I}$ is a $U \times U$ identity matrix, $\mathbf{H}^\dagger$ denotes transpose conjugate, and ρ is the average per-receiver-antenna signal-to-noise ratio (SNR).

The channel coefficients for each path are generated using the method in II-E, which produces MIMO channel matrices at different delays that are correlated both in time (Doppler spread) and space (antenna spacing) for each of the N channel paths. After superimposing all the six paths and sampling at a frequency 10 times the maximum Doppler frequency, a Discrete Fourier Transform (DFT) is performed that results in the MIMO channel frequency response at each sample time. The wideband capacity can then be calculated in the frequency domain on a bin by bin basis by computing the average over the frequency bins. The average (over time) wideband capacity for each channel profile over a fading distance of 40λ is computed and the CDF of the 1000 channel profile average capacities is what is plotted. The equal transmit power MIMO capacity with S data streams is compared to the beamforming to broadside of a single data stream. For the narrowband case the broadside beamforming capacity, which assumes approximate knowledge of the MS location) is given by:

$$C = \log_2 \left(\det \left[\mathbf{I} + \frac{\rho}{S} \mathbf{H}\mathbf{v}\mathbf{v}^\dagger\mathbf{H}^\dagger \right] \right) \qquad \text{bps/Hz} \qquad (28)$$

where $\mathbf{v}$ is an $S \times 1$ steering vector of all its elements equal to unity.

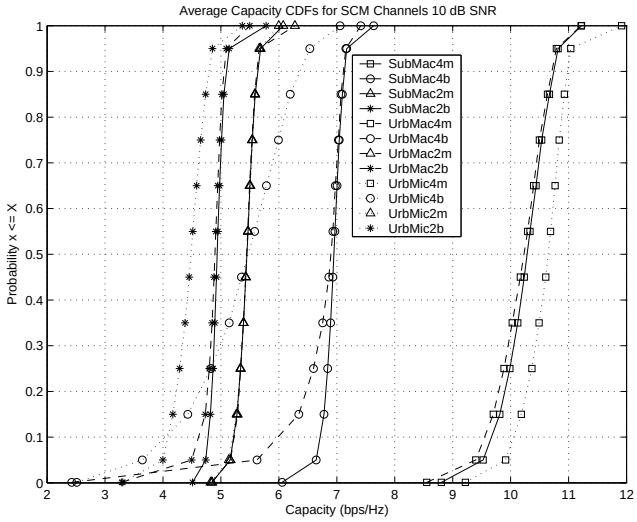

Fig. 7. CDFs of average capacities for the three channel environments and four array configurations when $SNR = 10dB$

The results are shown in Figs. 7 and 8, with a uniform MS antenna spacing of 0.5λ. For the 4×4 configurations, the average MIMO capacity is shown when the BS antenna spacing is 4λ ($SMac4m$, $UMac4m$, and $UMic4m$), and

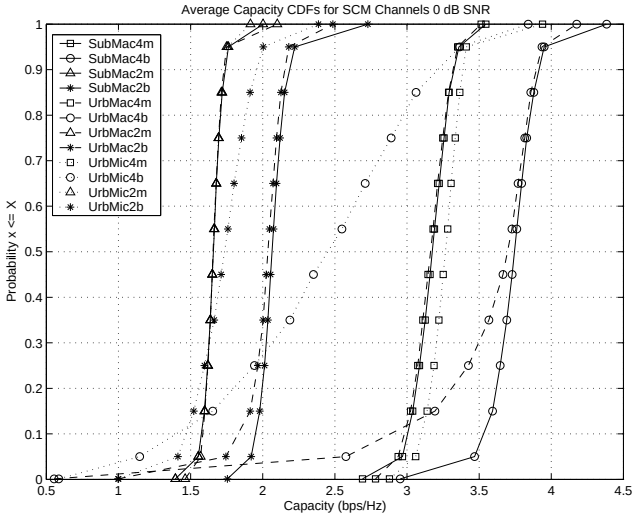

Fig. 8. CDFs of average capacities for the three channel environments and four array configurations when $SNR = 0dB$

the average broadside beamforming capacity is shown when the BS antenna spacing is 0.5λ ($SMac4b$, $UMac4b$, and $UMic4b$). For the 2×2 configurations, the average MIMO capacity is shown when the BS antenna spacing is 10λ ($SMac2m, UMac2m$, and $UMic2m$), and the average broadside beamforming capacity is shown when the BS antenna spacing is 0.5λ ($SMac2b$, $UMac2b$, and $UMic2b$). At the low SNR, $0dB$, and for the channels with higher spatial correlation (macrocells), the beamforming techniques appear to be advantageous to the MIMO approach [62]. The BS antenna spacings in all MIMO configurations are chosen so that the total length of the uniform linear array remains is comparable in all cases.

Recall that the macroscopic and mesoscopic parameters are computed once for each user for a given simulation run. The only parameters that need to be computed for each channel realization are the fast-fading coefficients at the microscopic level. For a given multipath and transmit/receive antenna pair, these coefficients are generated by summing $M = 20$ sinusoids, and this computation comparable in complexity to the well-known Jakes model [63] using M oscillators. The complexity of computing the complete MIMO channel per user for a large number of realizations is dominated by the computation of the fast-fading coefficients, and this complexity scales in proportionally with NSU. For a large-scale simulation with many users over thousands of time instances, the total number of arithmetic operations required for computing the coefficients in on the order of millions; therefore the complexity is easily manageable using any modern computer.

V. Summary and Conclusions

A unified spatiotemporal channel model framework was developed, which is applicable to multi-cell, system-level, simulations for up to 5MHz bandwidth. Particularly, it describes the channel properties in three scales (macro, meso-, and microscopic), and it specifies the dependencies between pathloss, temporal, and spatial physical parameters, their values, and the methods for implementing the model. It also provides modeling approaches for the special cases of far scatterer clusters, urban microcells, and urban canyon environments. The model also is extended to include the use of polarized antennas. While maintaining reasonable computational complexity, the model attempts to match the reported measurement data in the literature. Some examples of its output statistics are shown to illustrate the model's behavior.

Acknowledgments

The authors wish to acknowledge the comments and useful discussions with the other members of the Joint 3GPP/3GPP2 Spatial Channel Model (SCM) Ad-Hoc group.

References

[1] "Guidelines for Evaluation of Radio Transmission Technologies for IMT-2000," *Recommendation ITU-R M.1225*, 1997.

[2] "3GPP deployment aspects," *3GPP TR 25.943 V5.1.0*, June 2002.

[3] "1xEV-DV evaluation methodology - Addendum - V6," WG3/WG5 TSG-C 3GPP2, Tech. Rep., July 2001, available at: ftp://ftp.3gpp2.org /TSGC /Working/2001 /TSG-C_0108 /TSG-C-0801-Portland /WG5 /C50-20010820-026.

[4] H. Xu, D. Chizhik, H. Huang, and R. Valenzuela, "A wave-based wideband MIMO channel modeling technique," in *IEEE PIMRC*, vol. 4, Lisbon, Portugal, Sept. 2002, pp. 1626–1630.

[5] A. F. Molisch, M. Steinbauer, M. Toeltsch, E. Bonek, and R. Thoma, "Capacity of MIMO systems based on measured wireless channels," *IEEE J. Select. Areas Commun.*, vol. 20, pp. 561–569, 2002.

[6] D. Hampicke, M. Landmann, C. Schneider, G. Sommerkorn, R. Thoma, T. Fugen, J. Maurer, and W. Wiesbeck, "MIMO capacities for different antenna array structures based on double directional wide-band channel measurements," in *IEEE Proc. Vehicular Technology Conf., Fall*, 2002, pp. 180–184.

[7] C.-C. Chong, C.-M. Tan, D. I. Laurenson, S. McLaughlin, M. A. Beach, and A. R. Nix, "A new statistical wideband spatio-temporal channel model for 5-GHz band WLAN systems," *IEEE J. Select. Areas Commun.*, vol. 21, pp. 139–150, 2003.

[8] T. Zwick, C. Fischer, and W. Wiesbeck, "A stochastic multipath channel model including path directions for indoor environments," *IEEE J. Select. Areas Commun.*, vol. 20, pp. 1178–1192, 2002.

[9] Q. Spencer, B. Jeffs, M. Jensen, and A. Swindlehurst, "Modeling the statistical time and angle of arrival characteristics of an indoor multipath channel," *IEEE J. Select. Areas Commun.*, vol. 18, pp. 347–360, 2000.

[10] J. W. Wallace and M. A. Jensen, "Modeling the indoor MIMO wireless channel," *IEEE Trans. Antennas Propagat.*, vol. 50, pp. 591–599, 2002.

[11] A. Saleh and R. Valenzuela, "A statistical model for indoor multipath propagation," *IEEE J. Select. Areas Commun.*, vol. 5, no. 2, pp. 128–137, 1987.

[12] J. Fuhl, A. F. Molisch, and E. Bonek, "A unified channel model for mobile radio systems with smart antennas," *IEEE Proc. - Radar, Sonar and Navigation: Special Issue on Antenna Array Processing Techniques*, p. 145, Feb. 1998.

[13] O. Norklit and J. B. Andersen, "Diffuse channel model and experimental results for array antennas in mobile environments," *IEEE Trans. Antennas and Propagation*, vol. 46, pp. 834 –840, 1998.

[14] J. J. Blanz and P. Jung, "A flexibly configurable spatial model for mobile radio channels," *IEEE Trans. Commun.*, vol. 46, pp. 367–371, 1998.

[15] J. B. Liberti and T. S. Rappaport, "A geometrically based model for line-of-sight multipath radio channels," in *Proc. IEEE Vehicular Techn. Conf.*, 1996, pp. 844–848.

[16] P. Petrus, J. H. Reed, and T. S. Rappaport, "Geometrical-based statistical macrocell channel model for mobile environments," *IEEE Trans. Commun.*, vol. 50, pp. 495–502, 2002.

[17] A. Abdi and M. Kaveh, "A space-time correlation model for multielement antenna systems in mobile fading channels," *IEEE J. Select. Areas Commun.*, vol. 20, pp. 550–560, 2002.

[18] T. Svantesson, "A physical MIMO radio channel model for multi-element multi-polarized antenna systems," in *Proc. VTC fall*, 2001, pp. 1083–1087.

[19] R. M. Buehrer, S. Arunachalam, K. H. Wu, and A. Tonello, "Spatial channel model and measurements for IMT-2000 systems," in *IEEE Proc. 53rd Vehicular Technology Conf., Spring*, vol. 1, 2001, pp. 342–346.

[20] C. Oestges, V. Erceg, and A. J. Paulraj, "A physical scattering model for mimo macrocellular broadband wireless channels," *IEEE J. Select. Areas Commun.*, vol. 21, no. 5, pp. 721–729, 2003.

[21] J. H. Winters, "On the capacity of radio communications systems with diversity in Rayleigh fading environments," *IEEE J. Select. Areas Commun.*, vol. 5, pp. 871–878, June 1987.

[22] G. J. Foschini and M. J. Gans, "On limits of wireless communications in a fading environment when using multiple antennas," *Wireless Personal Communications*, vol. 6, pp. 311–335, 1998.

[23] A. L. Moustakas, H. U. Baranger, L. Balents, A. M. Sengupta, and S. H. Simon, "Communication through a diffusive medium: Coherence and capacity," *Science*, vol. 287, pp. 287–290, January 2000.

[24] D. Chizhik, F. Rashid-Farrokhi, J. Ling, and A. Lozano, "Effect of antenna separation on the capacity of BLAST in correlated channels," *IEEE Commun. Lett.*, vol. 4, no. 11, pp. 337–339, November 2000.

[25] J. P. Kermoal, L. Schumacher, K. Pedersen, P. E. Mogensen, and F. Frederiksen, "A stochastic MIMO radio channel model with experimental validation," *IEEE J. Select. Areas Commun.*, vol. 20, pp. 1211–1226, 2002.

[26] K. Yu, M. Bengtsson, B. Ottersten, D. McNamara, P. Karlsson, and M. Beach, "A wideband statistical model for NLOS indoor MIMO channels," in *IEEE Proc. Vehicular Technology Conf., Spring*, 2002, pp. 370–374.

[27] D. P. McNamara, M. A. Beach, and P. N. Fletcher, "Spatial correlation in indoor MIMO channels," in *IEEE Symp. on Personal, Indoor and Mobile Radio Comm.*, 2002, pp. 290–294.

[28] M. Lienard, P. Degauque, J. Baudet, and D. Degardin, "Investigation on MIMO channels in subway tunnels," *IEEE J. Select. Areas Commun.*, vol. 21, pp. 332–339, 2003.

[29] H. O. W. Weichselberger, M Herdin and E. Bonek, "A stochastic MIMO channel model with joint correlation of both link ends," *IEEE Transactions on Wireless Communications*, to appear.

[30] M. Steinbauer and A. F. Molisch, "Directional channel modelling," in *Wireless Flexible Personalized Communications*, L. Correia, Ed. J. Wiley, U.K., 2001, ch. 3.2, pp. 148–194.

[31] A. F. Molisch, H. Asplund, R. Heddergott, M. Steinbauer, and T. Zwick, "The COST259 directional channel model - I. Overview and Methodology," *IEEE Trans. Wireless Comm.*, p. accepted pending revisions, 2001.

[32] H. Asplund, A. A. Glazunov, A. F. Molisch, K. I. Pedersen, and M. Steinbauer, "The COST259 directional channel model - II. Macrocells," *IEEE Trans. Wireless Comm.*, p. submitted.

[33] A. F. Molisch, J. E. Dietert, R. Heddergott, M. Steinbauer, and T. Zwick, "The COST259 directional channel model - III. Micro- and Picocells," *IEEE Trans. Wireless Comm.*, p. to be submitted.

[34] V. Erceg, xy, x x, x x, x x, x x, and x x, "TGn channel model," *Doc IEEE 802.11-03/940r04*, Nov. 2003.

[35] H. Xu, D. Chizhik, H. Huang, and R. Valenzuela, "A generalized space-time multiple input multiple output (MIMO) channel model," *IEEE Trans. Wireless Communications*, vol. 3, pp. 966–975, May 2004.

[36] "Spatial channel model text v.7.0," Joint 3GPP/3GPP2 SCM AdHoc," SCM-135, Technical Report, August 19 2003, Available at: ftp://ftp.3gpp2.org /TSGC /Working /2003 /3GPP_3GPP2 _SCM_(Spatial_Modeling) /ConfCall-16-20030417/.

[37] E. Damosso and L. Correia, Eds., *Digital Mobile Radio Towards Future Generation Systems*. European Union, Luxemburg, 1994, available at http://www.lx.it.pt/cost231/.

[38] L. J. Greenstein, V. Erceg, Y. S. Ye, and M. V. Clark, "A new path-gain/delay-spread propagation model for digital cellular channels," *IEEE Trans. Veh. Technol.*, vol. 46, no. 2, pp. 477–485, May 1997.

[39] C. Cheon, G. Liang, and H. L. Bertoni, "Simulating radio channel statistics for different building environments," *IEEE J. Select. Areas Commun.*, vol. 19, no. 11, pp. 2191–2200, Nov. 2001.

[40] A. Algans, K. I. Pedersen, and P. E. Mogensen, "Experimental analysis of the joint statistical properties of azimuth spread, delay spread, and shadow fading," *IEEE J. Select. Areas Commun.*, vol. 20, no. 3, pp. 523–531, April 2002.

[41] N. C. Beaulieu, A. A. Abu-Dayya, and P. J. McLane, "Estimating the distribution of a sum of independent lognormal random variables," *IEEE Trans. Commun.*, vol. 43, no. 12, pp. 2869–2873, Dec. 1995.

[42] L. M. Correia, Ed., *Wireless Flexible Personalised Communications; COST 259: European Co-operation in Mobile Radio Research*. Chichester, UK: J. Wiley & Sons, 2001.

[43] C. Oestges, D. Vanhoenacker-Janvier, and B. Clerckx, "Wide-band simo 1x2 measurements and characterization of outdoor wireless channels at 1.9 ghz," *IEEE Trans. Veh. Technol.*, vol. 53, no. 4, pp. 1190–1202, 2004.

[44] J. Weitzen and T. J. Lowe, "Measurement of angular and distance correlation properties of log-normal shadowing at 1900 MHz and its application to design of PCS systems," *IEEE Trans. Veh. Technol.*, vol. 51, no. 2, pp. 265–273, March 2002.

[45] K. I. Pedersen, P. E. Mogensen, and B. H. Fleury, "A stochastic model of the temporal and azimuthal dispersion seen at the base station in outdoor propagation environments," *IEEE Trans. Veh. Technol.*, vol. 49, no. 2, pp. 437–447, March 2000.

[46] D. Reed, "Path characteristics for spatial channel model," Motorola, Joint 3GPP/3GPP2 SCM AdHoc Standards Contribution," SCM-041, August 1 2002, Available at: ftp://ftp.3gpp2.org /TSGC/Working /2002/3GPP_3GPP2_SCM _(Spatial_Modeling) /ConfCall-5-20020801/.

[47] M. Garry Hess, "A ray-based MIMO propagation model," 3GPP2 Standards Contribution," C50-SCM-20010820-027, August 2001, available at: ftp: //ftp.3gpp2.org /TSGC /Working /2001 /TSG-C_0108 /TSG-C-0801 -Portland /WG5/.

[48] S. Y. Seidel, T. S. Rappaport, S. Jain, M. L. Lord, and R. Singh, "Path loss, scattering and multipath delay statistics in four european cities for digital cellular and microcellular radiotelephone," *IEEE Trans. Veh. Technol.*, vol. 40, pp. 721–730, 1991.

[49] U. Martin, "Spatio-temporal radio channel characteristics in urban macrocells," *Proc. IEE Radar, Sonar Navigation*, vol. 145, no. 1, p. 42, 1998.

[50] A. Kuchar, J.-P. Rossi, and E. Bonek, "Directional macro-cell channel characterization from urban measurements," *IEEE Trans. Antennas Propagat.*, vol. 48, no. 2, pp. 137–146, Feb. 2000.

[51] T. S. Rappaport, S. Y. Seidel, and R. Singh, "900- MHz multipath propagation measurements for US digital cellular radiotelephone," *IEEE Trans. Veh. Technol.*, vol. 39, pp. 132–139, 1990.

[52] H. Asplund, A. F. Molisch, M. Steinbauer, and N. Mehta, "Clustering of scatterers in mobile radio channels - evaluation and modeling in the COST259 directional channel model," *Proc. ICC*, pp. 901–905, 2002.

[53] A. F. Molisch, "Effect of far scatterer clusters in MIMO outdoor channel models," *Proc. VTC Spring*, 2003.

[54] H. Foster, S. Dehghan, R. Steele, J. Stefanov, and H. Strelouhov, "Microcellular measurements and their prediction," *IEE Proceedings*, pp. 2/1–2/6, 1994.

[55] S. Kozono, T. Tsuruhara, and M. Sakamoto, "Base station polarization diversity reception for mobile radio," *IEEE Trans. Veh. Technol.*, vol. 33, no. 4, p. 301, November 1984.

[56] W. C. Y. Lee, *Mobile Communications Engineering: Theory and Practice*. New York: chap. 5, pp. 198-199, McGraw-Hill, 1998.

[57] R. G. Vaughan, "Polarization diversity in mobile communications," *IEEE Trans. Veh. Technol.*, vol. 39, no. 3, pp. 177–186, 1990.

[58] J. J. A. Lempiainen and J. K. Laiho-Steffens, "The performance of polarization diversity schemes at a base station in small/micro cells at 1800 MHz," *IEEE Trans. Veh. Technol.*, vol. 47, no. 3, pp. 1087–1092, August 1998.

[59] P. C. Eggers, I. Z. Kovacs, and K. Olesen, "Penetration effects on XPD with GSM1800 handset antennas, relevant for BS polarization diversity for indoor coverage," *Proc. VTC*, pp. 1959–1963, 1998.

[60] C. Oestges, V. Erceg, and A. J. Paulraj, "Propagation modeling of MIMO multipolarized fixed wireless channels," *IEEE Trans. Veh. Technol.*, vol. 53, no. 3, pp. 644–654, 2004.

[61] G. Calcev, "Polarization effects and path statistics," Motorola, Joint 3GPP/3GPP2 SCM AdHoc Standards Contribution," SCM-055, September 17 2002, available at: ftp://ftp.3gpp2.org /TSGC/Working /2002/3GPP _3GPP2_SCM _(Spatial_Modeling) /ConfCall-6-20020917/.

[62] A. L. Moustakas, S. H. Simon, and A. M. Sengupta, "MIMO capacity through correlated channels in the presence of correlated interferers and noise: A (not so) large N analysis," *IEEE Trans. Inform. Theory*, vol. 49, no. 10, pp. 2545–2561, Oct. 2003.

[63] W. C. Jakes, *Microwave Mobile Communications*. New Jersey: IEEE Press, 1974.

PLACE PHOTO HERE

George Calcev

PLACE PHOTO HERE

Dmitry Chizhik is a Member of Technical Staff in the Wireless Research Laboratory at Bell Labs, Lucent Technologies. He received a Ph.D. in Electrophysics at the Polytechnic University, Brooklyn, NY in 1991. His thesis work has been in ultrasonics and non-destructive evaluation. ' He joined the Naval Undersea Warfare Center, New London, CT where he did research in scattering from ocean floor, geoacoustic modeling and shallow water acoustic propagation. In 1996 he has joined Bell Laboratories, working on radio propagation modeling and measurements, using deterministic and statistical techniques. His recent work has been in measurement, modeling and channel estimation of MIMO channels. The results are used both for determination of channel-imposed bounds on channel capacity, system performance, as well as for optimal antenna array design. His research interests are in acoustic and electromagnetic wave propagation, signal processing and communications.

PLACE PHOTO HERE

Bo Göransson received his MSc in Electrical Engineering and applied physics from Linköping University in 1992 and his PhD from Royal Institute of Technology (KTH), Stockholm, Sweden in 1997, respectively. In 1998 he joined the research department at Ericsson Radio Systems AB, now Ericsson Research. He has been involved in research and standardization of multi antenna systems for WCDMA and its evolution. His research interests are in signal processing and its applications to wireless communications.

PLACE PHOTO HERE

Steven Howard (S'88-M'92) received a BS degree from the University of Connecticut, Storrs, CT, in 1979, an MS degree from Southern Methodist University, Dallas, TX, in 1981, and a PhD degree from Worcester Polytechnic Institute, Worcester, MA, in 1991. He is currently a Principal Engineer with Qualcomm, Concord MA, where he has been performing research and design of MIMO communication systems since 1999. During this time, he has participated in the Spatial Channel Model joint standardization group for 3GPP/3GPP2, and the Indoor MIMO WLAN Channel Models group for IEEE 802.11 TGn. He was Director of Measurement Systems with NextWave Telecom from 1996-1998. Prior to NextWave, he was at Raytheon Company for 14 years working on tactical military communication systems, and for 3 years at Texas Instruments working on working on radar and sonar signal processing systems.

PLACE PHOTO HERE

Howard Huang was born in Houston, Texas on March 17, 1969. He received a B.S.E.E degree from Rice University in 1991 and a Ph.D. in electrical engineering from Princeton University in 1995. Since graduating, he has worked at Bell Labs, Lucent Technologies, where he is currently a Distinguished Member of Technical Staff in the Center for Wireless and Broadband Access Networks. He has served as the rapporteur of the MIMO work item in the 3GPP standards, and his interests are in communication theory and MIMO system design.

PLACE PHOTO HERE

Achilles Kogiantis received the Diploma degree in Electrical Engineering from the University of Patras, Greece, in 1990, and the Ph.D. degree in Electrical Engineering from the University of Virginia, Charlottesville, VA, in 1994. From 1995 to 1997 he held an Assistant Professor position in the Electrical & Computer Engineering Department and the Center for Telecommunications Studies at the University of Louisiana, Lafayette, LA. Since 1997, he has been with the Wireless Advanced Technologies Laboratory, Lucent Technologies, Whippany, NJ, where he has been involved in various aspects of system design, performance analysis and algorithms development for CDMA systems. Particularly, he has studied the interaction of multiple antennas and scheduled packet data and the integration of MIMO in 3G. He took an active role in 3G standardization efforts on the definition of mixed circuit and packet data air-interfaces, transmit diversity, MIMO, and spatial channel modeling. His current interests include communications theory and system design, distributed spatial multiplexing and the broadcast channel, and adaptive antenna arrays.

PLACE PHOTO HERE

Andreas F. Molisch (S'89, M'95, SM'00, F'05) received the Dipl. Ing., Dr. techn., and habilitation degrees from the Technical University Vienna (Austria) in 1990, 1994, and 1999, respectively. From 1991 to 2000, he was with the TU Vienna, becoming an associate professor there in 1999. From 2000-2002, he was with the Wireless Systems Research Department at AT&T (Bell) Laboratories Research in Middletown, NJ. Since then, he has been a Senior Principal Member of Technical Staff with Mitsubishi Electric Research Labs, Cambridge, MA. He is also professor and chairholder for radio systems at Lund University, Sweden.

Dr. Molisch has done research in the areas of SAW filters, radiative transfer in atomic vapors, atomic line filters, smart antennas, and wideband systems. His current research interests are MIMO systems, measurement and modeling of mobile radio channels, and UWB. Dr. Molisch has authored, co-authored or edited four books (among them the recent textbook "Wireless Communications, Wiley-IEEE Press), eleven book chapters, some 85 journal papers, and numerous conference contributions.

Dr. Molisch is an editor of the IEEE Trans. Wireless Comm., co-editor of a recent special issue on MIMO and smart antennas in J. Wireless Comm. Mob. Comp., and co-editor of an upcoming IEEE JSAC special issue on UWB. He has been member of numerous TPCs, vice chair of the TPC of VTC 2005 spring, and will be general chair of ICUWB 2006. He has participated in the European research initiatives "COST 231", "COST 259", and "COST273", where he was chairman of the MIMO channel working group, and is also chairman of Commission C (signals and systems) of URSI (International Union of Radio Scientists). Dr. Molisch is a Fellow of the IEEE and recipient of several awards.

PLACE PHOTO HERE

Aris L. Moustakas (SM'04) received a B.S. degree in physics from Caltech in 1990 and M.S. and Ph.D. degrees in theoretical condensed matter physics from Harvard University in 1992 and 1996, respectively. In 1998, he joined Bell Labs, Lucent Technologies, NJ, first in the Physical Sciences Division and then also in the Wireless Advanced Technology Laboratory. Since 2005 he is an assistant professor at the Physics Dept. of the National Capodistrian University of Athens. His current research interests lie in the areas of multiple antenna systems, signal processing for smart antennas and the applications of statistical physics methods to the theory of communications.

PLACE PHOTO HERE

Doug Reed (M'81) received the B.S. and M.E. degrees in electrical engineering in 1981 and 1984 from the University of Texas at Arlington. He is a Distinguished Member of the Technical Staff at Motorola Labs in Ft. Worth, Texas where he works to develop next generation wireless systems. He is currently involved in the evolution of cellular standards in 3GPP and 3GPP2. His current research interests include: cellular system design, system simulations, propagation analysis, and channel modeling.

PLACE PHOTO HERE

Hao Xu (S'96-M'00) was born in Wuhan, China, in 1971. He received the B.S. and M.S. degrees from Moscow Power Engineering Institute and Technical University, Moscow, Russia, in 1994 and 1996, respectively. He received the Ph.D. degree from the Mobile and Portable Radio Research Group (MPRG) at Virginia Tech., Blacksburg, VA, in 2000.

From 2000 to 2003, he worked at Wireless Communications Research Laboratories and Wireless Advanced Technologies Laboratories, Bell Laboratories, Crawford Hill, NJ. His research at Bell Laboratories focused on MIMO channel characterization, capacity evaluation, and cellular network optimizations. Since October 2003, he has been with the Corporate R&D Systems Engineering Group at Qualcomm, San Diego, CA, where he is working on physical layer design for OFDM and CDMA systems.

In 2002, he received Bell Laboratories President's Gold Award for his contribution to the BLAST project. In 1999, Dr. Xu received the IEEE Communications Society Stephen O. Rice Prize Award for the best original journal article in the IEEE Transactions on Communications with Dr. G. Durgin and Dr. T. S. Rappaport. In 1989, as a result of his third place ranking in the national entrance examination to universities in China, he received Zhang Zhongzhi Prize Award from the University of Science and Technologies in China (USTC) and was awarded a six year fellowship by the Chinese government from 1989 to 1996. He has numerous publications and currently serves as an Associate Editor for IEEE TRANSACTIONS ON WIRELESS COMMUNICATIONS.